Development of MHD simulation capability for stellarators[1]

Carl Sovinec, Colin Guilbault, Brian Cornille, and Torrin Bechtel

Department of Engineering Physics
University of Wisconsin-Madison

Wistell Group Meeting, November 20, 2020

[1]Supported by US DOE grant DE-SC0018642.

Outline

- Objective for stellarator-centric developments
- Generalized geometry
- Magnetic representation
- Other points and next steps

The objective is a practical model for nonlinear stellarator MHD.

There are important questions regarding MHD dynamics in stellarators and torsatrons:

- Loss of equilibrium due to β-driven topology change from large Shafranov shift
- Symmetry-breaking instabilities that lead to soft β–limits

Some stellarator/torsatron configurations are possible with the standard NIMROD representation.

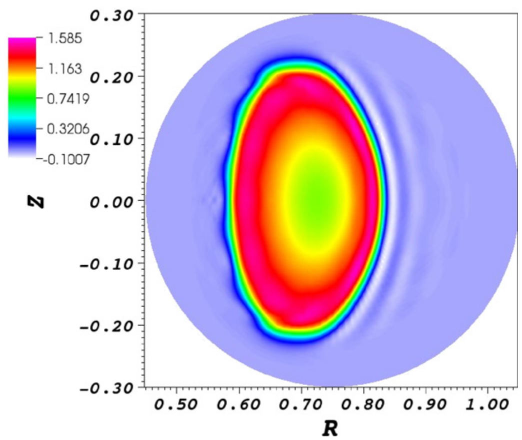

Mark Schlutt investigated startup MHD in CTH with applied loop voltage. [NF **52**, 103023 (2012)]

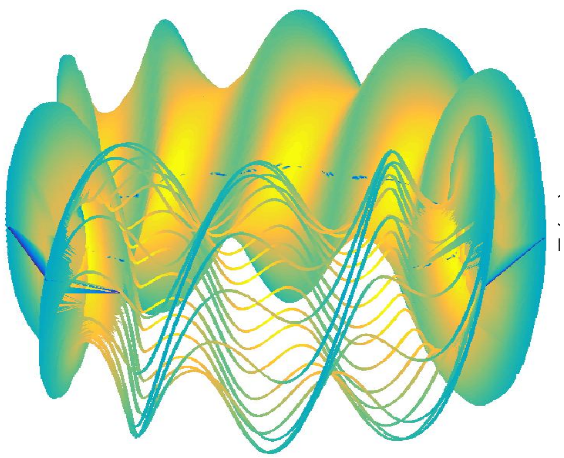

Torrin Bechtel investigates *p*-driven loss of equilibrium in an l = 2, N_p= 10 configuration.

- However, there are significant limitations:
  - Mesh and wall geometry are assumed to be axisymmetric.
  - Coil locations must be outside the axisymmetric domain.
  - Numerical convergence with helical coil fields is challenging.

Visco-resistive MHD with fluid closures will be the base model.

$$\frac{\partial n}{\partial t} + \nabla \cdot \left(n\mathbf{V} \right) = -\nabla \cdot \mathbf{\Gamma}_n$$

particle continuity with artificial diffusion

$$mn\left(\frac{\partial}{\partial t} + \mathbf{V} \cdot \nabla \right)\mathbf{V} = \mathbf{J} \times \mathbf{B} - \nabla (2nT) - \nabla \cdot \underline{\Pi} + \mathbf{S}_p$$

momentum density ($T_i = T_e = T$)

$$\frac{n}{\gamma - 1}\left(\frac{\partial}{\partial t} T + \mathbf{V} \cdot \nabla T \right) = -nT\nabla \cdot \mathbf{V} - \nabla \cdot \mathbf{q} + S_Q$$

temperature evolution

$$\frac{\partial \mathbf{B}}{\partial t} = -\nabla \times \left(\eta \mathbf{J} - \mathbf{V} \times \mathbf{B} \right)$$

Faraday's law & resistive MHD Ohm's

$$\mu_0 \mathbf{J} = \nabla \times \mathbf{B}$$

Ampere's law

- Extended-MHD systems will be developed after stellarator functionality is established.

Closure relations approximate plasma transport; sources include numerical corrections.

- Thermal conduction and viscous stress are anisotropic.
  - $\mathbf{q} = -n\left[\left(\chi_{\|} - \chi_{iso}\right)\hat{\mathbf{b}}\hat{\mathbf{b}} + \chi_{iso}\underline{\mathbf{I}}\right]\cdot\nabla T$
  - $\underline{\Pi} = \nu_{\|} mn\left(\underline{\mathbf{I}} - 3\hat{\mathbf{b}}\hat{\mathbf{b}}\right)\hat{\mathbf{b}}\cdot\underline{\mathbf{W}}\cdot\hat{\mathbf{b}} - \nu_{iso} mn\underline{\mathbf{W}}$ $\quad\underline{\mathbf{W}} = \nabla\mathbf{V} + \nabla\mathbf{V}^T - \frac{2}{3}\underline{\mathbf{I}}\nabla\cdot\mathbf{V}$
- Equations include numerical error-correcting terms.
  - Diffusive particle flux: $\mathbf{\Gamma}_n = -D_n\nabla n + D_h\nabla\nabla^2 n$
  - Momentum correction: $\mathbf{S}_p = m\mathbf{V}\nabla\cdot\mathbf{\Gamma}_n$
  - Ohmic and viscous heating + energy correction:

$$S_Q = \frac{1}{2}\left(\eta J^2 - \underline{\Pi}:\nabla\mathbf{V}\right) + \left(\frac{T}{\gamma-1} - \frac{mV^2}{4}\right)\nabla\cdot\mathbf{\Gamma}$$

Fields are expanded into steady and evolving components.

- Steady components are treated as prescribed data and should satisfy $\partial/\partial t \to 0$ to be self-consistent.

$$\frac{\partial \tilde{n}}{\partial t} + \nabla \cdot \left(n_s \tilde{\mathbf{V}} + \tilde{n} \mathbf{V}_s + \tilde{n} \tilde{\mathbf{V}} \right) = -\nabla \cdot \mathbf{\Gamma}_n$$

$$m\left(n_s + \tilde{n}\right)\left(\frac{\partial}{\partial t} \tilde{\mathbf{V}} + \mathbf{V}_s \cdot \nabla \tilde{\mathbf{V}} + \tilde{\mathbf{V}} \cdot \nabla \mathbf{V}_s + \tilde{\mathbf{V}} \cdot \nabla \tilde{\mathbf{V}} \right) + m \tilde{n} \mathbf{V}_s \cdot \nabla \mathbf{V}_s$$
$$= \mathbf{J}_s \times \tilde{\mathbf{B}} + \tilde{\mathbf{J}} \times \mathbf{B}_s + \tilde{\mathbf{J}} \times \tilde{\mathbf{B}} - 2\nabla\left(n_s \tilde{T} + \tilde{n} T_s + \tilde{n} \tilde{T} \right) - \nabla \cdot \underline{\tilde{\Pi}} + \mathbf{S}_p$$

$$\frac{\left(n_s + \tilde{n}\right)}{\gamma - 1}\left(\frac{\partial}{\partial t} \tilde{T} + \mathbf{V}_s \cdot \nabla \tilde{T} + \tilde{\mathbf{V}} \cdot \nabla T_s + \tilde{\mathbf{V}} \cdot \nabla \tilde{T} \right) + \frac{\tilde{n}}{\gamma - 1} \mathbf{V}_s \cdot \nabla T_s$$
$$= -n_s T_s \nabla \cdot \tilde{\mathbf{V}} - \left(n_s \tilde{T} + \tilde{n} T_s + \tilde{n} \tilde{T} \right) \nabla \cdot \left(\mathbf{V}_s + \tilde{\mathbf{V}} \right) - \nabla \cdot \tilde{\mathbf{q}} + S_Q$$

$$\frac{\partial \tilde{\mathbf{B}}}{\partial t} = -\nabla \times \left(\eta_s \tilde{\mathbf{J}} + \tilde{\eta} \mathbf{J}_s + \tilde{\eta} \tilde{\mathbf{J}} - \mathbf{V}_s \times \tilde{\mathbf{B}} - \tilde{\mathbf{V}} \times \mathbf{B}_s - \tilde{\mathbf{V}} \times \tilde{\mathbf{B}} \right) + \mathbf{S}_B$$

Generalizing NIMROD's geometry is critical.

- NIMROD's 2D spectral element/1D Fourier representation is retained.
- New: Expand geometric information in toroidal Fourier harmonics.

$$R(\xi,\eta,\zeta) = R_0(\xi,\eta) + \sum_{n=1}^{N}\left[R_n(\xi,\eta)e^{in\zeta} + c.c.\right]$$

$$Z(\xi,\eta,\zeta) = Z_0(\xi,\eta) + \sum_{n=1}^{N}\left[Z_n(\xi,\eta)e^{in\zeta} + c.c.\right]$$

$$\phi(\xi,\eta,\zeta) = \zeta + \phi_0(\xi,\eta) + \sum_{n=1}^{N}\left[\phi_n(\xi,\eta)e^{in\zeta} + c.c.\right]$$

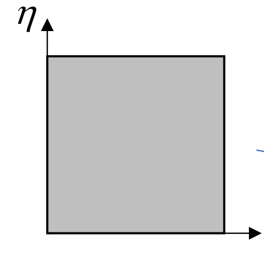

Standard 2D element.

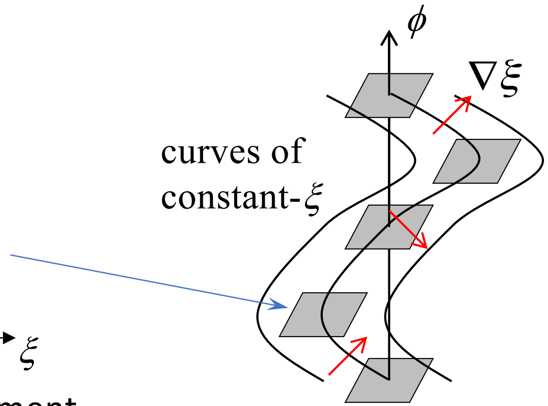

Illustration of a single element at different ζ-coordinate values.

- The generalized toroidal angle ζ implies:

$$\nabla\xi\cdot\nabla\zeta \neq 0 \quad , \quad \nabla\eta\cdot\nabla\zeta \neq 0 \quad \text{and when} \quad \zeta \neq \phi, \;\; \nabla\zeta \neq \frac{1}{R}\hat{\phi} \;\; .$$

Linear-geometry computations demonstrate the new capability.

- Example course meshes show the generalization:

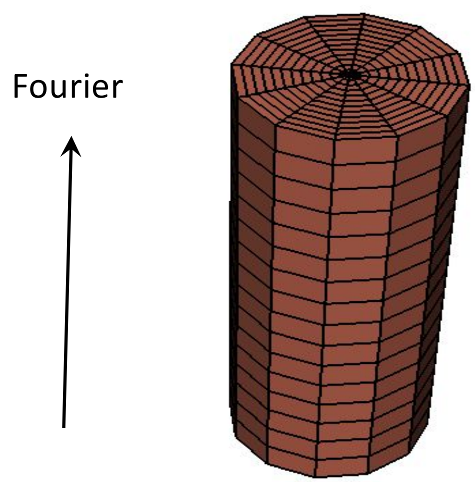

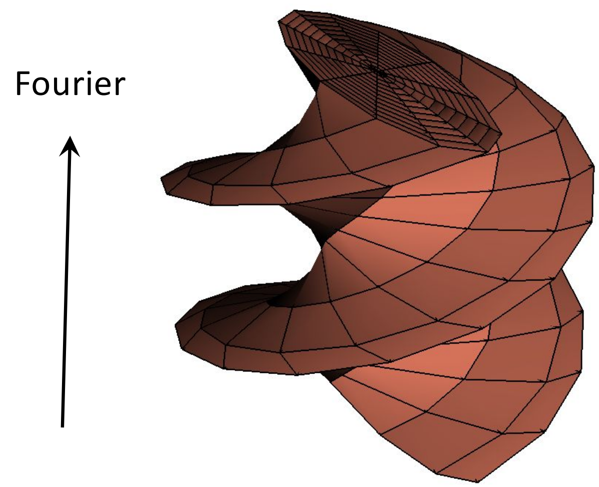

Conventional NIMROD meshes are uniform in the Fourier-expanded direction.

New meshing can follow 3D flux-surface shaping (also in toroidal geometry).

We consider convergence on helical anisotropic diffusion.

- The computation is $\frac{1}{\gamma-1}\frac{\partial T}{\partial t} = \nabla \cdot \left[\left(\chi_{||} - \chi_{iso}\right)\hat{\mathbf{b}}\hat{\mathbf{b}} + \chi_{iso}\mathbf{I}\right] \cdot \nabla T + S_Q$, run to steady state with uniform *T* along the boundary.
- Fixed helical field is: $\mathbf{B} = \nabla\left[AI_l\left(N_p r/R\right)\cos\left(l\theta - N_p z/R\right) + z\right]$
- The configuration considered here has $l = 2$ and ($N_p = 1$, $R = 4$) or ($N_p = 2$, $R = 8$) for $0.19 < \iota < 0.25$.
- The *X*-points are located where

  $\mathbf{B} \cdot \nabla r = 0$ and $\mathbf{B} \cdot \nabla\left(l\theta - N_p\, z/R\right) = 0$
- Plotting shows that the *X*-points occur at $r = 3.46$.

Thermal energy is transported to the open-field region.

- The “cat eye” confinement region of this *l* = 2 case is clear with both meshes.

Straight Mesh

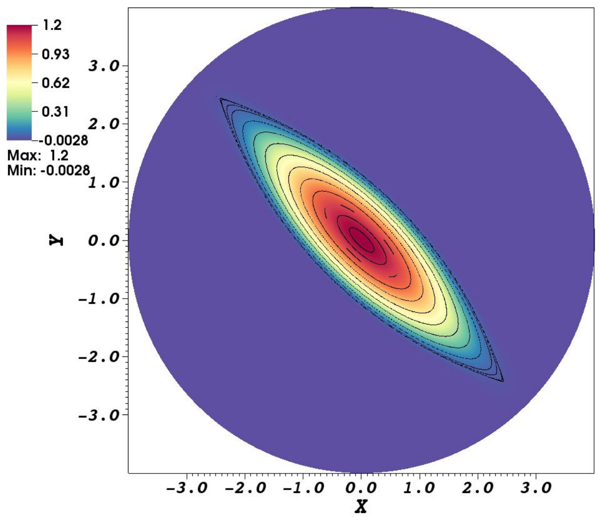

Magnetic Poincaré plot overlaying computed temperature for N_ϕ=32, pd=5, and mx=my=32.

Helical Mesh

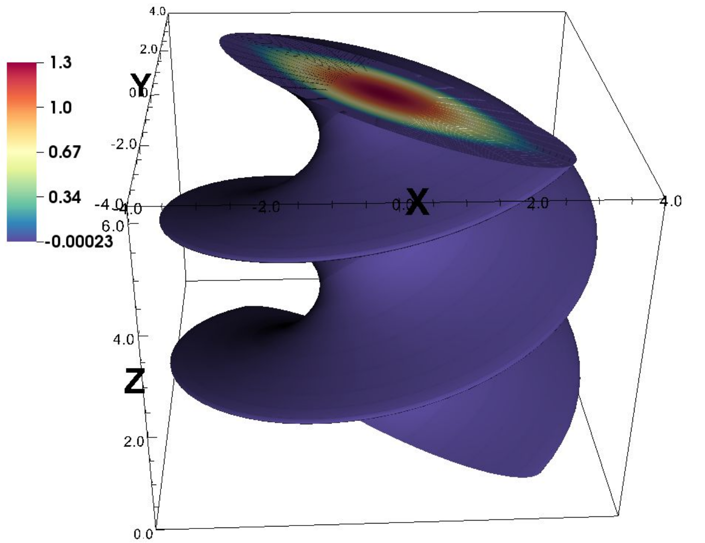

Computed temperature with pd=4, mx=my=32 on a shaped helical mesh.

The meshing strongly influences numerical convergence.

- Normalized parameters have $S_Q = 4,\ \chi_{||} = (2/3)\times 10^6,\ \chi_{iso} = 2/3$.
- Here, pd = degree of polynomials in mx × my polar meshes of elements.

Straight Circular Mesh

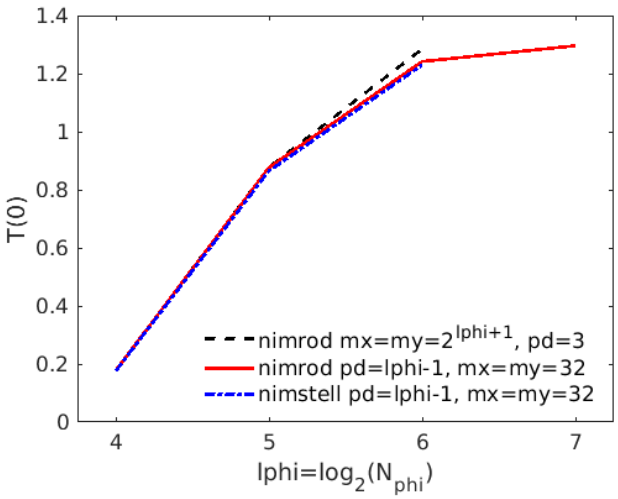

Central-*T* vs. poloidal and axial resolution that are varied simultaneously.

Helical Circular Mesh

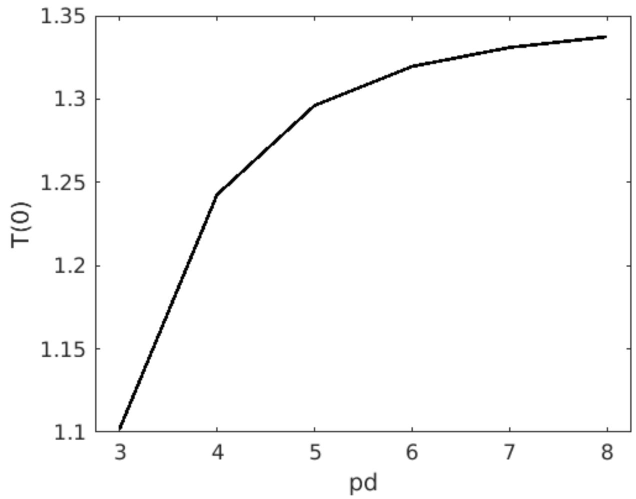

Central-*T* vs. poloidal resolution with Fourier $0 \leq n \leq 1$ (N_{phi}=4) only.

Helical Elliptical Mesh

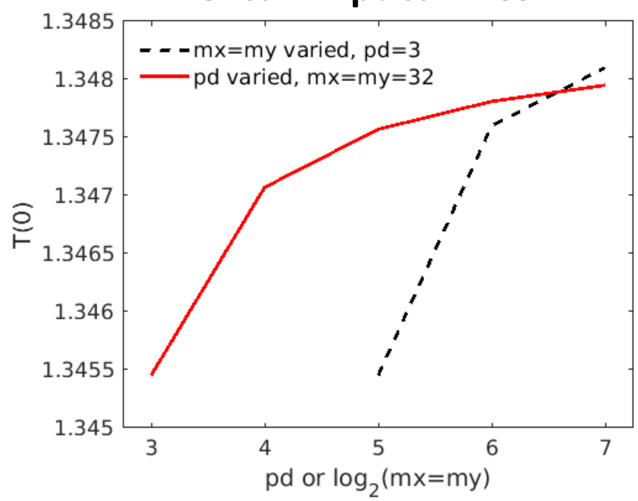

Central-*T* vs. poloidal resolution with $0 \leq n \leq 1$ only.

Using magnetic vector-potential can avoid divergence error.

- The Nedelec *H*(curl) elements[3] maintain flexibility with respect to polynomial bases.

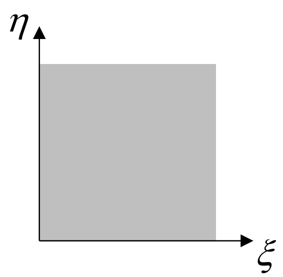

Standard 2D element.

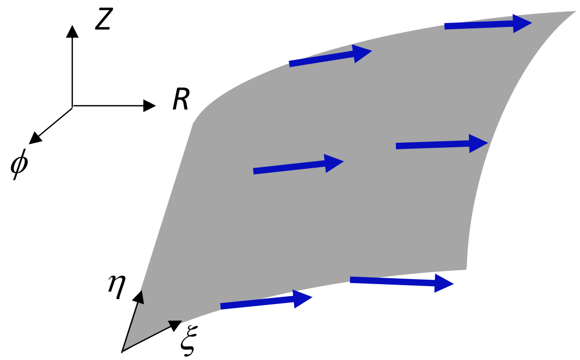

Linear-quadratic nodal
$\sigma(\xi)\lambda(\eta)\nabla\xi$ basis vectors.

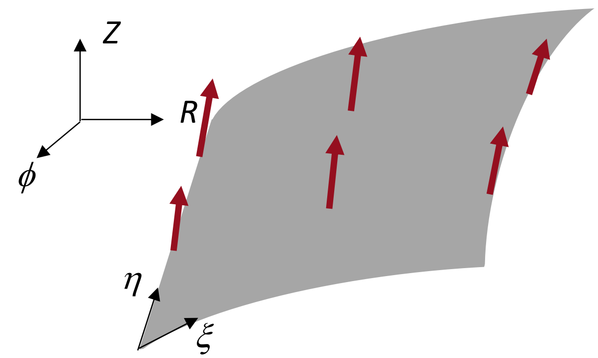

Quadratic-linear nodal
$\lambda(\xi)\sigma(\eta)\nabla\eta$ basis vectors.

- The third basis vector is $\lambda(\xi)\lambda(\eta)\nabla\zeta$.
- Tangential components are continuous; normal components are not.
- The normal component of their curl is continuous.

[3]J. C. Nedelec, Numerische Mathematik **35**, 315 (1980).

Differential operators in time-dep. MHD and magnetostatics differ.

- Magnetostatic computations use **A** in *H*(curl) elements; gauge set with H^1 elements.[4]
  - The double curl leads to a mathematically stable weak formulation.

Linear $\mathbf{V}_0$=0, ideal MHD

$$\rho_0 \frac{\partial \boldsymbol{v}}{\partial t} = \nabla \cdot (\boldsymbol{B}_0 \nabla\times\boldsymbol{a} + \nabla\times\boldsymbol{a}\boldsymbol{B}_0) - \nabla(\boldsymbol{B}_0 \cdot \nabla\times\boldsymbol{a} + p)$$

$$\frac{\partial p}{\partial t} = -\gamma P_0 \nabla \cdot \boldsymbol{v} - \boldsymbol{v} \cdot \nabla P_0$$

$$\frac{\partial \boldsymbol{a}}{\partial t} = \boldsymbol{v}\times\boldsymbol{B_0} - \nabla\chi$$

$$\nabla^2\chi = C\nabla \cdot \boldsymbol{a}$$

Magnetostatics

$$\nabla\times\frac{1}{\mu}\nabla\times\boldsymbol{a} = \boldsymbol{j}$$

$$\frac{1}{\mu\epsilon^2}\nabla \cdot \epsilon\boldsymbol{a} = \chi$$

- The double-curl arises in MHD only with non-zero resistivity.

[4]Y.-L. Li, S. Sun, Q. I. Dai, and W. C. Chew, IEEE Trans. Mag. **51**, 7002306 (2015).

We test different formulations with 1D cylindrical ideal-MHD eigenvalue computations.[5]

- Elements are 1D in r ; θ and z are Fourier.
- Formulations with different dependent variables are readily programmed.
- Radial expansions for each dependent variable are set at runtime.
- In cylindrical geometry, 1D H(curl) elements have:
  - Discontinuous expansions for A_r of 1 degree lower than for rA_θ and A_z
  - Continuous expansions of rA_θ and A_z of the same degree

[5]C. R. Sovinec, J. Comput. Phys. **319**, 61 (2016).

The cylindrical eigenvalue computations support the use of *H*(curl).

- Results shown here have degree(rA_θ, A_z, ϕ) = degree(**V**, p, A_r)+1 .

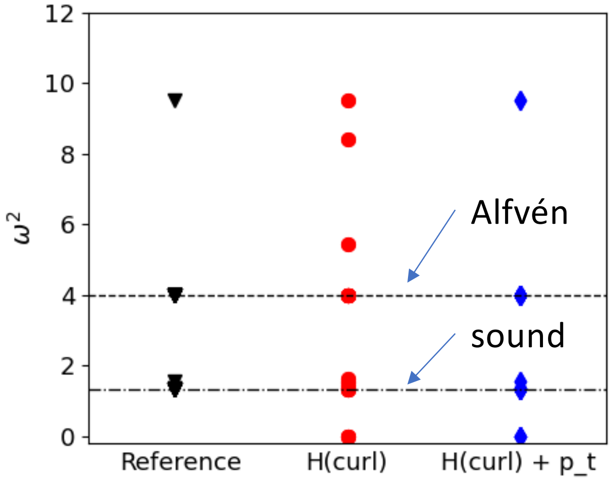

Eigenvalues for (m=1,*k*=2) with uniform $\boldsymbol{B}_0 = B_0\hat{\boldsymbol{z}}$, ρ_0, and P_0.

- The *H*(curl) computations have 3 elements in *r*.

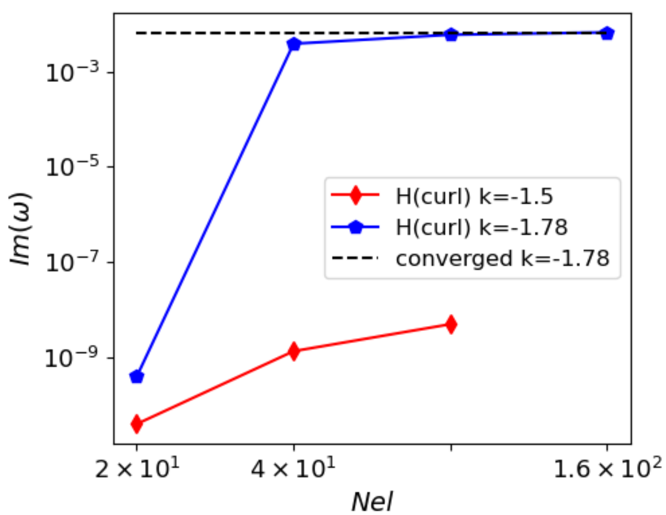

Equilibria with peaked P_0 have bad curvature: *k*=-1.5->stable; *k*=-1.78->un.

- Convergence is from stable side.

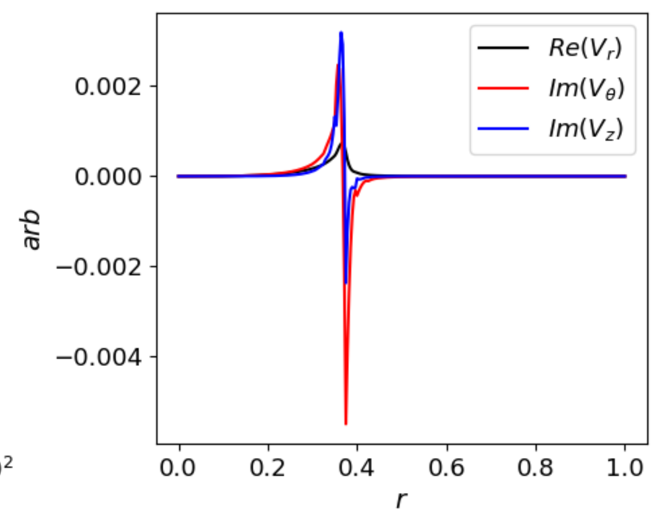

Eigenfunction of unstable mode is localized.

- **A** in *H*(curl) without resistivity admits 0-frequency modes.

Other gauge conditions produce more errors.

- Previous uses Coulomb via damping:

$$\frac{\partial \boldsymbol{a}}{\partial t} = \boldsymbol{v}\times\boldsymbol{B_0} - \nabla\chi$$

$$\nabla^2\chi = C\nabla\cdot\boldsymbol{a}$$

$$\frac{\partial\nabla\cdot\boldsymbol{a}}{\partial t} = \nabla\cdot\boldsymbol{v}\times\boldsymbol{B_0} - C\nabla\cdot\boldsymbol{a}$$

- Alternative 1 uses Weyl:

$$\frac{\partial \boldsymbol{a}}{\partial t} = \boldsymbol{v}\times\boldsymbol{B_0}$$

- Alternative 2 uses Coulomb via diffn:

$$\frac{\partial \boldsymbol{a}}{\partial t} = \boldsymbol{v}\times\boldsymbol{B_0} - \nabla\chi$$

$$\chi = C_2\nabla\cdot\boldsymbol{a}$$

$$\frac{\partial\nabla\cdot\boldsymbol{a}}{\partial t} = \nabla\cdot\boldsymbol{v}\times\boldsymbol{B_0} - \nabla^2 C_2\nabla\cdot\boldsymbol{a}$$

  - Needs **A** in H^1.

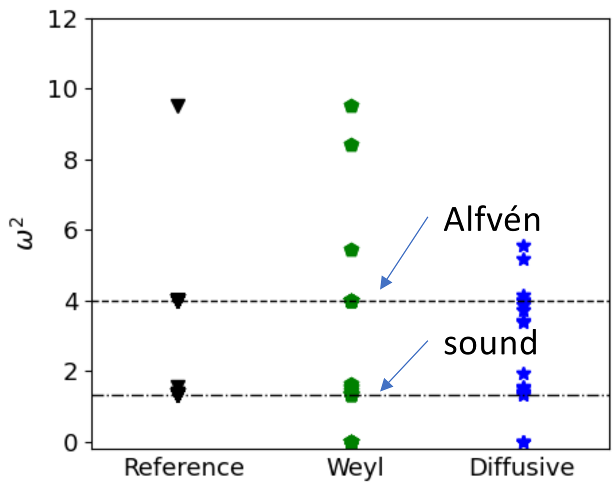

Eigenvalues for (m=1,k=2) with uniform $\boldsymbol{B}_0 = B_0\hat{\boldsymbol{z}}$, ρ_0, and P_0.

- Weyl has many more 0-frequency modes.

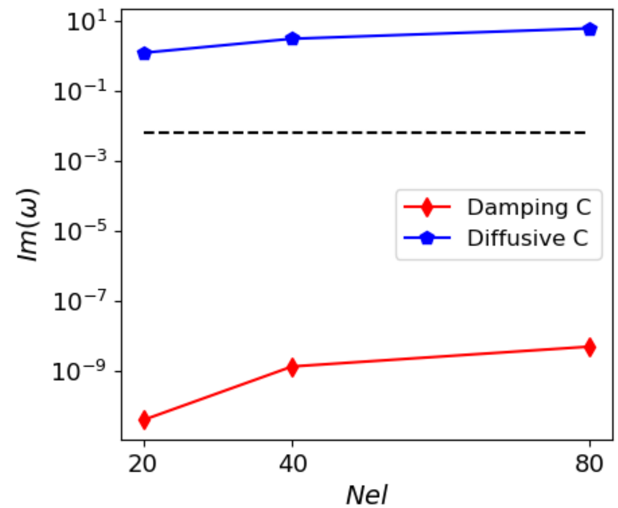

The diffusive approach allows the k=-1.5 case (blue) grow faster than the converged k=-1.78 (dashed).

The choice of vector-potential representation affects convergence.

- Cases shown here use:

$$\frac{\partial \boldsymbol{a}}{\partial t} = \boldsymbol{v} \times \boldsymbol{B_0} - \nabla \chi$$

$$\nabla^2 \chi = C \nabla \cdot \boldsymbol{a}$$

$$\frac{\partial \nabla \cdot \boldsymbol{a}}{\partial t} = \nabla \cdot \boldsymbol{v} \times \boldsymbol{B_0} - C \nabla \cdot \boldsymbol{a}$$

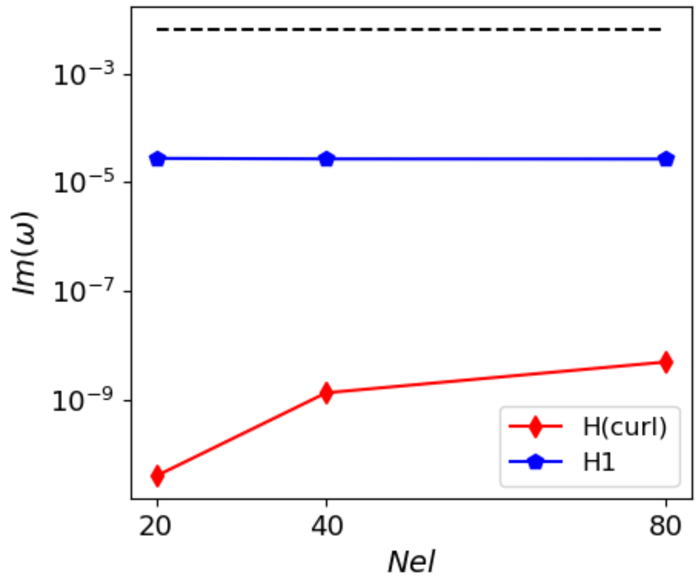

Using H^1 instead of H(curl) leads to a weakly unstable mode in physically stable conditions.

Other project aspects are in development.

- Advanced preconditioners for algebraic solves are being investigated.
  - Present NIMROD approach is block-diagonal in Fourier.
  - Extending cyclic reduction to include Fourier coupling is effective.[6]
- Pre-processing of equilibria will accept VMEC output.

[6] C. R. Sovinec, NIMROD Team Meeting, Aug. 21-23 (2019). [https://nimrodteam.org/meetings]

Conclusions and Next Steps

- The generalized NIMROD representation will facilitate stellarator applications.
- Divergence-free stellarator-MHD is feasible with **A** in *H*(curl).

- Next steps:
  - Implementing *H*(curl) **A**-representation in NIMSTELL branch
  - Reading VMEC output for pre-processing